Advances in Nano Research, *Vol. 15, No. 1 (2023) 59-65*
https://doi.org/10.12989/anr.2023.15.1.059

Studying the influences of mono-vacancy defect and strain rate on the unusual tensile behavior of phosphorene NTs

Hooman Esfandyari[1a], AliReza Setoodeh[*1], Hamed Farahmand[2], Hamed Badjian[1] and Greg Wheatley[3]

[1]*Department of Mechanical and Aerospace Engineering, Shiraz University of Technology, Shiraz 71555, Iran*
[2]*Department of Mechanical Engineering, Kerman Branch, Islamic Azad University, Kerman, Iran*
[3]*College of Science and Engineering, James Cook University, Townsville QLD Australia*

(*Received April 13, 2022, Revised December 5, 2022, Accepted December 6, 2022*)

Abstract. In this present article, the mechanical behavior of single-walled black phosphorene nanotubes (SW-αPNTs) is simulated using molecular dynamics (MD). The proposed model is subjected to the axial loading and the effects of morphological parameters, such as the mono-vacancy defect and strain rate on the tensile behavior of the zigzag and armchair SW-αPNTs are studied as a pioneering work. In order to assess the accuracy of the MD simulations, the stress-strain response of the current MD model is successfully verified with the efficient quantum mechanical approach of the density functional theory (DFT). Along with reproducing the DFT results, the accurate MD simulations successfully anticipate a significant variation in the stress-strain curve of the zigzag SW-αPNTs, namely the knick point. Predicting such mechanical behavior of SW-αPNTs may be an important design factor for lithium-ion batteries, supercapacitors, and energy storage devices. The simulations show that the ultimate stress is increased by increasing the diameter of the pristine SW-αPNTs. The trend is identical for the ultimate strain and stress-strain slope as the diameter of the pristine zigzag SW-αPNTs enlarges. The obtained results denote that by increasing the strain rate, the ultimate stress/ultimate strain are respectively increased/declined. The stress-strain slope keeps increasing as the strain rate grows. It is worth noting that the existence of mono-atomic vacancy defects in the (12,0) zigzag and (0,10) armchair SW-αPNT structures leads to a drop in the tensile strength by amounts of 11.1% and 12.5%, respectively. Also, the ultimate strain is considerably altered by mono-atomic vacancy defects.

Keywords: DFT; energy storage devices; knick point; mono-vacancy defect; single-walled beta phosphorene nanotubes; strain rate; molecular dynamics

1. Introduction

Two-dimensional materials such as graphene (Novoselov *et al*. 2009, Lee *et al*. 2008) boron nitride (Zhi *et al*. 2009, Golberg *et al*. 2010) and MoS_2 (Radisavljevic *et al*. 2011, Liu *et al*. 2012) have been attracted excessive attention in recent years due to their excellent electrical, thermal and mechanical properties. Guo *et al*. (2014) investigated the electronic properties of phosphorene nanoribbons, phosphorene nanotubes (NTs) and multilayer phosphorene. Ebrahimi *et al*. (2019b) studied the thermal buckling analysis of embedded grapheme-oxide powder-reinforced nanocomposite plates. Shi *et al*. (2016) considered the dynamic behavior of a black phosphorous and carbon nanotube composite system. Safaei *et al*. (2019) examined the axial buckling behavior of single-layered grapheme sheets using shear deformation theory. Jam *et al*. (2022) investigated on the crack propagation in carbon doped polycrystalline boron-nitride nanosheets using molecular dynamics simulation. Venkateshalu *et al*. (2022) reviewed the properties, synthesis techniques and the supercapacitive nature of phosphorene. Also Pang *et al*. (2018) studied the applications of phosphorene and black phosphorus in energy conversion and storage devices. According to the superior mechanical properties of two-dimensional single-layer black phosphorus termed phosphorene, plenty of research has been conducted to obtain the mechanical behavior of this structure (Sorkin and Zhang 2016). Phosphorene is a semiconductor with a 1.5 eV band-gap and high carrier mobility (Qiao *et al*. 2014) larger than semi-metallic graphene (Geim and Novoselov 2007). These properties create an extensive potential for phosphorene to be applied in nano-electric mechanical devices, e.g., transistors (Buscema *et al*. 2014), gas sensors (Kou *et al*. 2014), solar cells (Deng *et al*. 2014), and advanced batteries (Li *et al*. 2015).

Deformation in the atomic structure of two-dimensional materials is an essential factor affecting the physical properties of such materials. The fabrication and stability of SW-αPNTs and phosphorene nanostructures are firstly examined by Guan *et al*. (2014). In this regard, Fei and Yang (2014) found that the electron mobility of black phosphorus can be tuned by applying an in-plane strain. Moreover, phosphorene shows superior structural flexibility along the armchair direction resulting from the large building curvatures (Wang *et al*. 2016). Also, the DFT simulations demonstrates that the crystal phase of black phosphorous exhibits an anisotropic mechanical behavior (Setoodeh and Farahmand 2017).

*Corresponding author, Ph.D.,
E-mail: setoodeh@sutech.ac.ir; asetood@yahoo.com
[a]Ph.D. Student, E-mail: h.esfandyari@sutech.ac.ir

ISSN: 2287-237X (Print), 2287-2388 (Online)

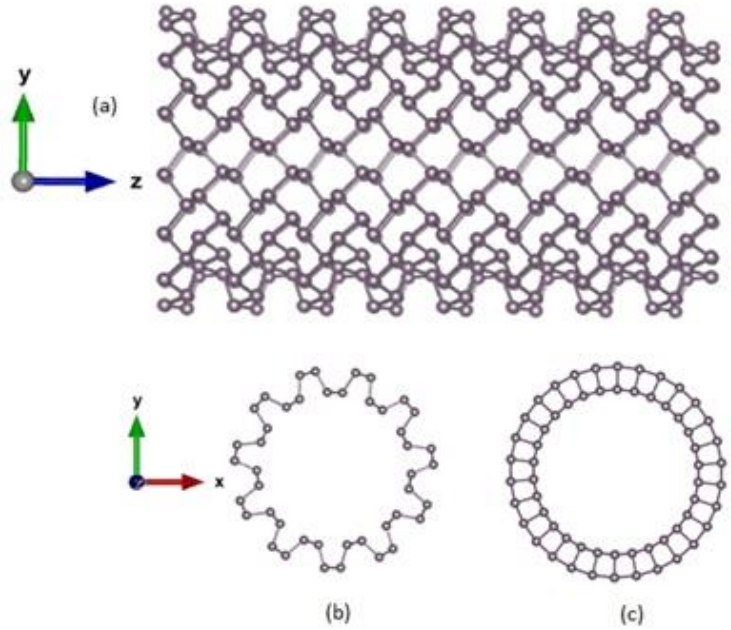

Fig. 1 The illustration of (a) SW-αPNT, (b) armchair (0,11), (c) zigzag (15,0)

From the other point of view, SW-αPNTs, as their pioneer counterparts, i.e., carbon nanotubes (CNTs), have recently been attracted excessive attention due to their superior mechanical, thermal, and electrical properties (Nguyen and Le 2018).

Due to such rapid progress in the development and potential application of αW-βPNTs, studying the mechanical behavior and material properties of such nanotubes is highly significant. It is worth noting that this structure is more stable when covered or terminated by single-layer carbon atoms such as grapheme-nanotube hybrids (Cai *et al*. 2016). Using the MD method, it was found that the deformation and failure of SW-αPNTs are highly anisotropic (Liao *et al*. 2016). In this research, it was found that the failure stress enhances from 7.3 to 10 GPa when the tube diameter increases from 1.1to 7.2nm for the case of armchair SW-αPNTs. In comparison, the ultimate strength of zigzag nanotubes alters from 2.6 to 3.8 GPa by increasing the tube diameter from 2 to 7.5nm. Ansari *et al*. (2017) presented a DFT coupled with a finite element method to study the mechanical properties of zigzag phosphorene nanotubes. Chen *et al*. (2017) investigated the mechanical properties of SW-αPNTs at atmospheric pressure by assuming two specific cross-sectional areas namely, a hollow tube and an equivalent solid cylinder, to estimate the mechanical properties. On the other hand, due to the minimum energy level of the SW-αPNT structure, various atomic defects appear in the phosphorene structure during its fabrication process (Sha *et al*. 2016). Accordingly, it was concluded that atomic vacancies induce local stress concentration and cause early bond-breaking and significant degradation of the mechanical properties of the material. Thus, studying the atomic vacancies is essential for extracting the mechanical properties of the structure (Liu *et al*. 2017). Zhu *et al*. (2020) investigated the thermal conductivity of phosphorus nanotubes anisotropy using molecular dynamics simulation. Hatam *et al*. (2021) studied the shear properties and tensile strength anisotropy of monolayer black phosphorene by molecular dynamics method. Aghdasi *et al*. (2021) presented elastic and plastic characteristics of monolayer phosphorene under atomic adsorption by the density functional theory.

Remarkably, in the current study, an exact MD simulation is established to predict the tensile behavior of pristine and mono-vacancy defected SW-αPNTs. Meanwhile, the unusual knick point in the tensile stress-strain curve of the nanostructure is observed, which was already predicted merely by DFT simulations. Moreover, the influences of morphological parameters such as the diameter of zigzag and armchair SW-αPNTs are studied by applying different strain rates. Eventually, the effects of the aforementioned parameters on the tensile behavior of the mono-vacancy defected SW-αPNTs are also investigated.

2. Computational method

Molecular dynamics is a prevalent and accurate methodology for investigating the physical movement of atoms and molecules based on Newtonian equations of motion considering interatomic interactions (Badjian and Setoodeh 2017). Accordingly, MD simulation is adopted to study the tensile behavior of SW-αPNTs. The puckered structure of SW-αPNT is shown in Fig. 1. In order to model the interaction forces between the atoms, the Stillinger-Weber (SW) potential field (Jin 2015) is utilized to describe the mechanical properties of SW-αPNTs. The open-source Large-scale Atomic/Molecular Massively Parallel Simulator (LAMMPS) software package (Plimpton 1995) is used to implement the MD simulations.

The periodic boundary condition is s*et al*ong the axial direction of SW-αPNTs. Herein, a time step of 0.5 fs is used

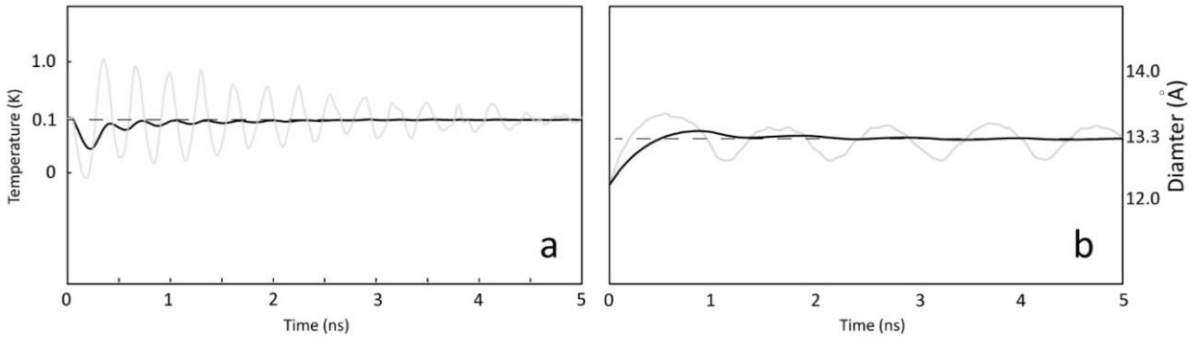

Fig. 2 Optimization and thermodynamic stability test of phosphorene nanotube; a) Stability of temperature, b) Stability of diameter

for the integration of the equations of atomic motion in the molecular dynamics simulations and the chosen time step is sufficiently small as the system energy is well conserved. The equations of motion through time have been solved using the Velocity-Verlet integration algorithm. The Nose-Hoover thermostat NVT ensemble is performed to keep the temperature, volume and the total number of atoms constant during the simulation. Moreover, the temperature is employed close to 0 K (0.1 K) in this paper to minimize collisions between atoms and remove any thermal stress during the simulation process. It is worth noting that the relaxation process is the essential step before applying any loading. This helps the structure reach the equilibrium state before extracting the output results. Therein, the conjugate gradient method is utilized doing this favor.

The strain is defined as the relative length change of the simulation box along the axial direction ($\varepsilon_Z = \Delta L/L_Z$). In order to calculate the stress, the interlayer spacing of phosphorene is taken as the thickness of an SW-αPNT, which is commonly assumed to be 0.524 nm [20]. Thus, Young's modulus (Y) of the structure can be calculated using the Eq. (1).

$$Y = \frac{1}{At}\frac{\partial^2 E}{\partial[\ln(1+\varepsilon_e)]^2} \quad (1)$$

where t is the thickness, A is the initial surface, E is the strain energy, and ε_e denotes the normal engineering strain along the loading direction (e).

3. Results and discussion

At first, the tensile behavior of the pristine and mono-vacancy defected SW-αPNTs is investigated at the strain rate of 0.004 ps^{-1} during the preceding atomistic simulations, unless otherwise is stated. According to the different morphology of SW-αPNTs, discussions about the tensile behavior of the nanotube are categorized into two separate sections: SW-αPNTs with the zigzag chiral index and those with the armchair configuration. Subsequently, the variation of the SW-αPNTs tensile properties with different diameters and strain rates are studied. Optimization and thermodynamic stability test before starting the simulation are very important in molecular dynamics. Therefore, optimization and thermodynamic stability tests of phosphorene nanotube are demonstrated in Fig. 2. In this simulation, the total time is considered to be as 5(ns).

3.1 Zigzag SW-αPNT

The unusual tensile behavior of the zigzag SW-αPNTs is first discussed. To validate the codes, the tensile behavior of pristine SW-αPNT is depicted in Fig. 3. The length of the SW-αPNT is 3.371nm with 480 atoms. Simultaneously, the MD results are evaluated with those obtained using the DFT simulation reported by Sorkin and Zhang (2016). As illustrated in Fig. 3, the stress-strain results are in an excellent agreement with those of Sorkin and Zhang (2016), and more significantly, the present model is capable of accurately predicting the knick point on the tensile behavior. The knick point occurs at stress and strain levels of 2.2 GPa and 0.12, respectively. The deformation behavior of the resulted nanotube before loading and at the fracture point is illustrated in Fig. 4.

After validating the simulation, the tensile behavior of the pristine SW-αPNTs under variable diameter sizes is displayed in Fig. 5. As the electronic properties of PNTs can be tuned from semiconducting to metallic by applying strain or electric field and different energy of bandgap can be achieved according to different loadings exerted by electrical field (Guo *et al*. 2014), the effect of uniaxial loading was discussed in this paper. The behaviors of PNTs under straining, in particular, their deformation and failure mechanisms and their critical strain and stress, are crucial to be comprehensively studied for their beneficial role in future nano-mechanical devices (Sorkin and Zhang 2016). For instance, the PNT can operate with high structural stability when deploys as a rotor with rotational frequency (Shi *et al*. 2016), wherein different deformation mechanisms are identified in the structure.

According to Fig. 5, as the diameter of this structure increases in SW-αPNT, the energy of bandgaps rises. The same discussion was also noted in Ref. (Guo *et al*. 2014). Thus, the extracted stress-strain curve was calculated by measuring the length of the bonds as a function of applied tensile strain with different diameters, which led us to find the total potential energy and force of the generated nanostructure.

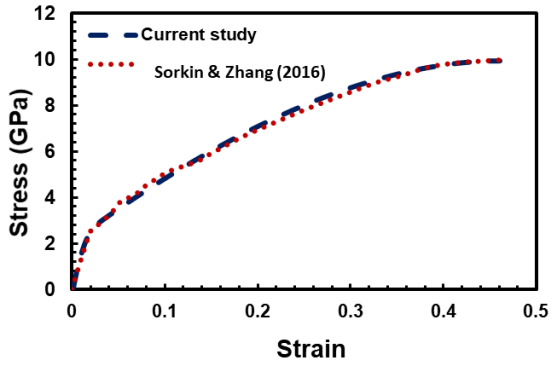

Fig. 3 Stress-strain curve for (15,0) pristine zigzag SW-αPNT under tensile loading

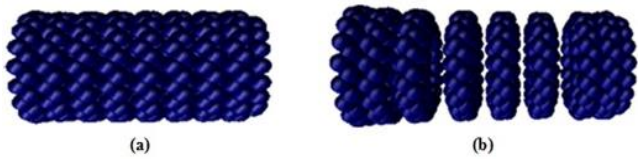

Fig. 4 The deformation behavior of SW-αPNT, (a) before loading; (b) failure

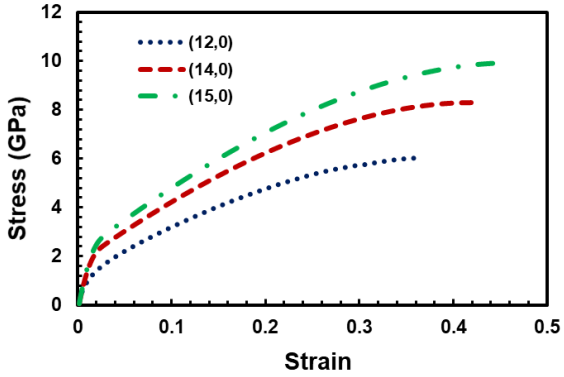

Fig. 5 Tensile stress-strain curves for pristine zigzag SW-αPNTs with various diameters

It is observed that the unexpected knick point appears on the stress-strain curves for different diameter sizes and that the knick point occurs at higher strains when the diameter increases. The significant phenomenon of knick point results from the alternation of the atomic bond angles. The results show that by increasing the diameter of the selected pristine SW-αPNT increases considerably the tensile strength of the nanostructure from 6.038 GPa up to 9.935 GPa. In fact by increasing the diameter, the number of atoms increases. Hence, the potential force between the atoms becomes stronger, and subsequently, the tensile strength increases. At the same time, the fracture strain alters from 0.361 up to 0.460 for the zigzag morphologies under consideration. Also by increasing the diameter of the pristine zigzag SW-αPNT, the stress-strain slope is increased.

Fig. 6 presents the effect of strain rate on the tensile behavior of the pristine zigzag SW-αPNTs. Obviously, the ultimate strength and stress-strain slope increase as the strain rate grows. Results show that with the strain rate increment of the pristine zigzag SW-αPNTs, the ultimate strain is decreased. Increasing strain rate does not affect the knick point position in terms of strain.

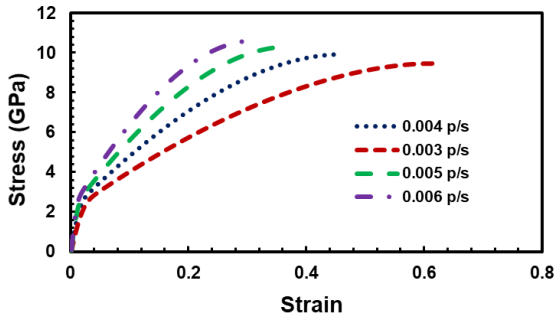

Fig. 6 Effects of strain rate on tensile behavior of (15,0) pristine zigzag SW-αPNTs

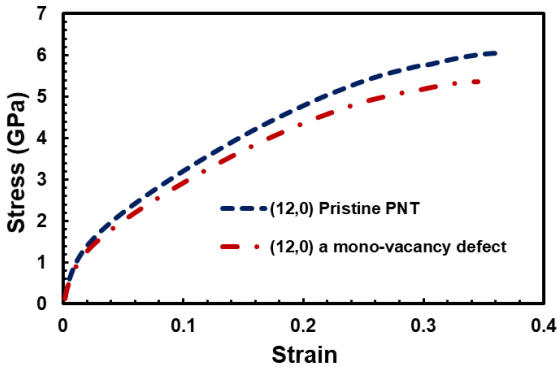

Fig. 7 Stress-strain curves of pristine and defective SW-αPNTs in zigzag direction

Table 1 Effect of strain rates on the tensile properties of (12,0) SW-αPNTs with mono-vacancy defect

Strain rate (p/s)	Ultimate strength (GPa)	Fracture strain
0.003	4.912	0.471
0.004	5.367	0.345
0.005	5.640	0.281
0.006	5.818	0.232

The tensile behavior of the defected (12,0) SW-αPNT is discussed in Fig. 7. It is seen that the ultimate strength dramatically reduces by an amount of 11.1% for the case of missing a single atom at the mid-part of the zigzag SW-αPNTs. In the defect region, the force between atoms is weakened which leads to a lower mechanical strength. One can understand that the elastic modulus of the defected nanotube remains almost unchanged. Results denote that by implementing a mono-atomic vacancy defect in the structure of zigzag SW-αPNT, the ultimate strain value is diminished. The stress-strain slope and knick point position were not affected with the addition of the mono-atomic vacancy defect. The influences of strain rates on the tensile properties of the (12,0) SW-αPNTs with the mono-vacancy defects are reported in Table 1, It can be noted that the increase of strain rate leads to an increase of the ultimate stress and perversely decreases the ultimate strain.

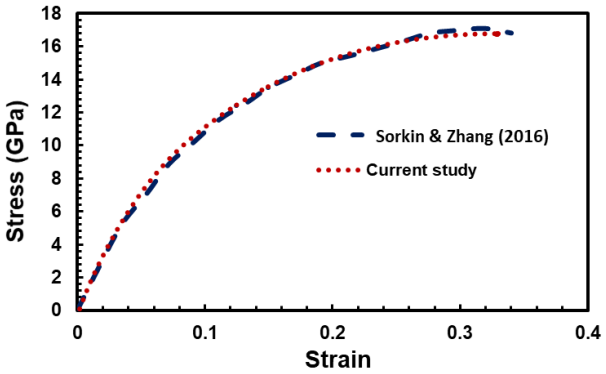

Fig. 8 Stress-strain curve for (0,11) pristine armchair SW-αPNTs under tensile loading

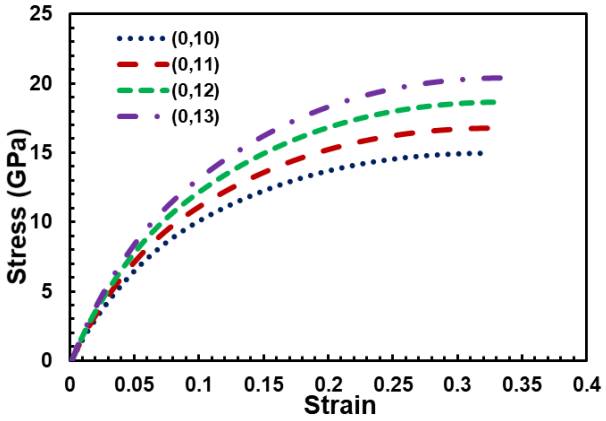

Fig. 9 Tensile stress-strain curves for pristine armchair SW-αPNTs with various diameters

3.2 Armchair SW-αPNT

To investigate whether the armchair SW-αPNTs behave analogously to corresponding zigzag nanotubes in tensile loading, similar simulations are performed in this section. Accordingly, the validation of the MD model is observed from the stress-strain curve of the (0,11) pristine SW-αPNTs under tensile loading as represented in Fig. 8. The length of the nanotube is 2.475nm with 352 atoms. Again, a good agreement is achieved between the current MD simulation and the DFT result (Sorkin and Zhang 2016). It is worth noting that the sudden change in the slope of the stress-strain curve as previously predicted for the zigzag nanotubes has not happened here.

The variations of tensile properties of the pristine SW-αPNT with different nanotube diameters are illustrated in Fig. 9. It can be seen that the ultimate strength of the nanotube significantly increases from 14.943 GPa to 20.428 GPa, while the fracture strain enhances from 0.325 up to 0.339. Actually, by increasing the diameter of phosphorene nanotube, the number of atoms increases. So the force between the atoms becomes stronger and consequently, the tensile strength increases. Also, stress-strain slopes are less affected by increasing diameter of pristine armchair SW-αPNTs.

In the next step, the effect of altering the strain rate on the mechanical behavior of pristine armchair SW-αPNT is

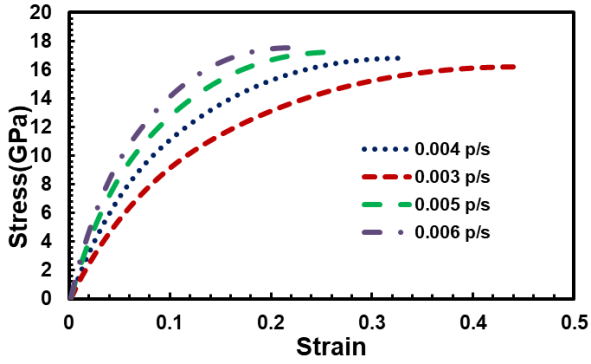

Fig. 10 Effects of strain rate on tensile behavior of (0,11) pristine armchair SW-αPNTs

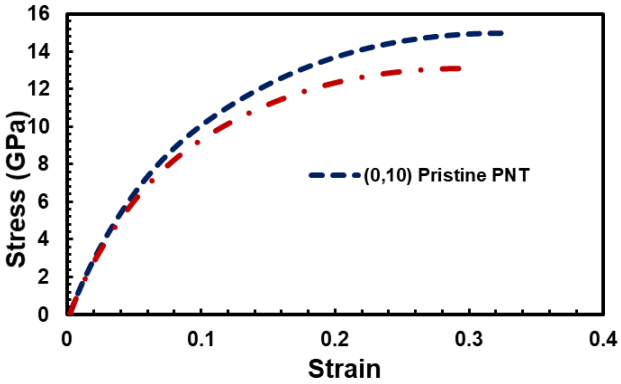

Fig. 11 Stress-strain curves of pristine and defective armchair SW-αPNTs

Table 2 Effect of strain rates on the tensile properties of (0,10) SW-αPNTs with mono-vacancy defect

Strain rate (p/s)	Ultimate strength (GPa)	Fracture strain
0.003	12.639	0.398
0.004	13.069	0.297
0.005	13.389	0.237
0.006	13.647	0.198

discussed in Fig. 10. One can find out that increasing the strain rate leads to an appreciable increase/decrease of the ultimate strength/fracture strain. The variation is more dominant for the fracture strain as observed previously for the nanotubes with zigzag chiral index. Results show that by increasing the strain rate of pristine armchair SW-αPNT, the stress-strain slope is increased significantly.

Eventually, the effect of mono-atomic vacancy defect in the middle length of the armchair SW-αPNT is discussed. As it is depicted in Fig. 11, a single mono-atomic vacancy defect greatly diminishes the tensile strength of the material in the armchair direction. The results indicate that such a defect reduces the ultimate strength and fracture strain of the simulated armchair SW-αPNT by 12.52% and 8.61%, respectively. Meanwhile, Young's modulus of the defected nanotube remains almost the same. To clarify the behavior of armchair SW-αPNTs with mono-vacancy defects, the influences of different strain rates on the ultimate strength and fracture strain of (0,10) nanotubes are reported in Table

2, It is concluded that the an increase of strain rate from 0.003 to 0.006 ps^{-1} leads to increase/decrease of the ultimate strength/fracture strain by amounts of 8% and 50.2%. It can also be noted that the reduction of fracture strain due to the increase of strain rate for zigzag SW-αPNTs is more prominent in comparison to the armchair nanotubes with identical diameters.

4. Conclusions

In this paper, the tensile behavior of SW-αPNTs is simulated using an accurate molecular dynamic simulation. The Stillinger-Weber interatomic potential field is utilized to represent the interatomic forces. As the most important result of the present work, the sudden change in the slope of the stress-strain curve of zigzag SW-αPNTs at the knick point is precisely anticipated as unusual mechanical behavior. In the following, the main results of our simulation tests are briefly presented.

• By increasing the diameter of the pristine zigzag SW-αPNTs, the ultimate stress, strain and stress-strain slope are increased significantly. The interesting unusual behavior for the knick point is observed when the diameter increases. Our results show that the knick point occurs at higher strains when the diameter increases.

• After studying the pristine armchair SW-αPNTs, it is observed that the ultimate stress enhances by increasing the diameter size. There is no knick point observed in this case and the stress-strain slope and ultimate strain are almost unchanged.

• Our results indicate that with the strain rate increment of the pristine zigzag SW-αPNTs, the ultimate stress and stress-strain slope are increased. Adversely, the fracture stain value is decreased by increasing strain rate. Increasing the strain rate does not affect the knick point position in terms of the strain.

• The findings of the present study for pristine armchair SW-αPNTs exhibit similar behavior to the results of the zigzag counterparts. The ultimate stress and stress-strain slope are enhanced with strain rate increment. Also, the ultimate strain values are reduced by increasing the strain rate.

• As one of our case studies, by implementing a mono-atomic vacancy defect in the structures of zigzag and armchair SW-αPNTs, the ultimate stress and strain values are diminished. The stress-strain slope is not affected by addition of the mono-vacancy defect. Interestingly, the knick point related to the zigzag nanostructure is less affected by the structure change.

References

Aghdasi, P., Ansari, R., Rouhi, S., Yousefi, S., Goli, M. and Soleimani, H.R. (2021), "Investigating elastic and plastic characteristics of monolayer phosphorene under atomic adsorption by the density functional theory", *Physica B*, **600**, 412603. https://doi.org/10.1016/j.physb.2020.412603.

Ansari, R., Shahnazari, A. and Rouhi, S. (2017), "A density-functional-theory-based finite element model to study the mechanical properties of zigzag phosphorene nanotubes", *Physica E*, **88**, 272-278. https://doi.org/10.1016/j.physe.2017.01.022.

Badjian, H. and Setoodeh, A.R. (2017), "Improved tensile and buckling behavior of defected carbon nanotubes utilizing boron nitride coating-A molecular dynamic study", *Physica B*, **507**, 156-163. https://doi.org/10.1016/j.physb.2016.12.006.

Buscema, M., Groenendijik, D.J., Steele, A.G., Zant, H.S.J. and Gomes, A. (2014), "Photovoltaic effect in few-layer black phosphorus PN junctions defined by local electrostatic gating", *Nature Commun.*, **5**, 4651. https://doi.org/10.1038/ncomms5651.

Cai, K., Wan, J., Yang, L. and Wei, N. (2016), "Mechanical behavior of composite double wall nanotubes from carbon and phosphorus", *Mater. Sci.*, **1**, 1607. https://doi.org/10.1039/C7CP01274H.

Chen, W.H., Yu, C.F., Chen, I.C. and Cheng, H.C. (2017), "Mechanical property assessment of black phosphorene nanotube using molecular dynamics simulation", *Comput. Mater. Sci.*, **133**, 35-44. https://doi.org/10.1016/j.commatsci.2017.03.008.

Deng, X.Y., Luo, Z., Conrad, N.J., Liu, Y., Gong, Y.J., Najmaei, S., Ajayan, P.M., Lou, J., Xu, X.F. and Ye, P.D. (2014), "Black phosphorus-monolayar MoS2 van der waals heterojunction p-n diode", *ACS Nano*, **8**, 8292-8299. https://doi.org/10.1021/nn5027388.

Ebrahimi, F., Nouraei, M., Dabbagh, A. and Rabczuk, T. (2019b), "Thermal buckling analysis of embedded graphene-oxide powder-reinforced nanocomposite plates", *Adv. Nano Res.*, **7**(5), 293-310. https://doi.org/10.12989/anr.2019.7.5.293.

Fei, R. and Yang, L. (2014), "Strain-engineering the anisotropic electrical conductance of few layer black phosphorus", *Nano Lett*, **14**, 2884-2889. https://doi.org/10.1021/nl500935z.

Geim, K.A. and Novoselov, K.S. (2009), "The rise of graphene", *Nanosci. Technol.*, **6**, 11-19. https://doi.org/10.1142/9789814287005_0002.

Golberg, D., Bando, Y., Huang, Y., Terao, T., Mitome, M., Tang, C. and Zhi, C. (2010), "Boron nitride nanotubes and nanosheets", *ACS Nano*, **4**, 2979-2993. https://doi.org/10.1021/nn1006495.

Guan, J., Zhu, Z. and Tomanek, D. (2014), "High stability of faceted nanotubes and fullerenes of multi-phase layered phosphorus: A computational study", *Phys. Rev. Lett.*, **113**, 226801. https://doi.org/10.1103/PhysRevLett.113.226801.

Guo, H., Lu, N., Dai, J., Wu, X. and Zeng, X.C., (2014), "Phosphorene nanoribbons, phosphorus nanotubes, and van der Waals multilayers", *J. Phys. Chem. C*, **118**(25), 14051-14059. https://doi.org/10.1021/jp505257g.

Hatam, S., Mohammadi, H. and Rajabpour, A. (2021), "Tuning shear mechanical properties and tensile strength anisotropy of monolayer black phosphorene: A molecular dynamics study", *Materialstoday*, **26**, 101796. https://doi.org/10.1016/j.mtcomm.2020.101796.

Jam, A., Jam, N., Izadifar, M.R. and Rabczuk, T. (2022), "Molecular dynamics study on the crack propagation in carbon doped polycrystalline boron-nitride nanosheets", *Comput. Mater. Sci.*, **203**, 111066. https://doi.org/10.1016/j.commatsci.2021.111066.

Jin-Wu, J. (2015), "Paramitrization of Stillinger-Weber potential based on valevce force field model: Application to single layer MoS2 and black phosphorus", *Nanotechnology*, **26**, 315706. https://doi.org/10.1088/0957-4484/26/31/315706.

Kou, Z.L., Frauenheim, T. and Chen, C.F. (2014), "Phosphorene as a superior gas sensor: Selective adsorption and distinct I-V response", *Phys. Chem. Let.t*, **5**, 2675-2681. https://doi.org/10.1021/jz501188k.

Lee, C., Wei, X. and Kysar, J.W. (2008), "Measurement of the elastic properties and intrinsic strength of monolayer graphene",

Science, **321**, 385-388. https://doi.org/10.1126/science.1157996.

Liao, X., Hao, F., Xiao, H. and Chen, X. (2016), "Effects of intrinsic strain on the structural stability and mechanical properties of phosphorene nanotubes", *Nanotechnology*, **27**, 215701. https://doi.org/10.1115/IMECE2016-65911.

Li, W.F., Yang, Y., Zhang, G. and Zhang, Y.W. (2015), "Ultrafast and directional diffusion of lithium in phosphorene for high-performance lithium-ion battery", *Nano Lett*, **15**, 1691-1697. https://doi.org/10.1021/nl504336h.

Liu, H., Neal, A.T. and Ye, P.D. (2012), "Channel length scaling of MoS2 MOSFETs", *ACS Nano*, **6**, 8563-8569. https://doi.org/10.1021/nn303513c.

Liu, P., Pei, Q.X., Huang, W. and Zhang, Y.W. (2017), "Mechanical properties and fracture behaviour of defective phosphorene nanotubes under uniaxial tension", *J. Phys. D*, **50**(48), 485303. https://doi.org/10.1088/1361-6463/aa8f66.

Nguyen, V.T. and Le, M.Q. (2018), "Compressive buckling of black phosphorene nanotubes: an atomistic study", *Mater. Res. Exp.*, **5**(4), 045024. https://doi.org/10.1088/2053-1591/aaba53.

Novoselov, K.S., Geim, A.K., Morozov, S.V., Jiang, D., Zhang, Y., Dubonos, S.V., Grigorieva, I.V. and Firsov, A.A. (2004), "Electric field effect in atomically thin carbon films", *Science*, **306**, 666-669. https://doi.org/10.1126/science.1102896.

Pang, J., Bachmatiuk, A., Yin, Y., Trzebicka, B., Zhao, L., Fu, L., Mendes, R.g., Gemming, T., Liu, Z. and Rummeli, M.H. (2018), "Applications of phosphorene and black phosphorus in energy conversion and storage devices", *Adv. Energy Mater.*, **8**, 1702093. https://doi.org/10.1002/aenm.201702093.

Plimpton, S. (1995), "Fast parallel algorithms for short range molecular dynamics", *J. Comput. Phys.*, **117**, 1-19. https://doi.org/10.1006/jcph.1995.1039.

Qiao, J., Kong, X., Hu, X .Z., Yang, F. and Ji, W. (2014), "High mobility trasport anisotropy and linear dichroism in few-layer black phosphorus", *Nature Commun.*, **5**, 4475. https://doi.org/10.1038/ncomms5475.

Radisavljevic, B., Radenovic, A., Brivio, J., Giacometti, I.V. and Kis, A. (2011), "Single-layer MoS2 transistors", *Nature Nanotech.*, **6**, 147-150. https://doi.org/10.1038/nnano.2010.279.

Safaei, B., Khoda, F.H. and Fattahi, A.M. (2019), "Non-classical plate model for single-layered graphene sheet for axial buckling", *Adv. Nano Res.*, **7**(4), 265-275. https://doi.org/10.12989/anr.2019.7.4.265.

Setoodeh, A.R. and Farahmand, H. (2017), "Nonlinear modeling of crystal system transition of black phosphorus using continuum-DFT model", *J. Phys. Codensed Matter*, **30**, 035901. http://doi.org/10.1088/1361-648X/aa99f7.

Sha, Z.D., Pei, Q.X., Zhang, Y.Y. and Zhang, Y.W. (2016), "Atomic vacancies significantly degrade the mechanical properties of phosphorene", *Nanotechnology*, **27**, 315704. https://doi.org/10.1088/0957-4484/27/31/315704.

Shi, J., Cai, H., Cai, K. and Qin, Q.H., (2016), "Dynamic behavior of a black phosphorus and carbon nanotube composite system", *J. Phys. D.*, **50**(2), p.025304. https://doi.org/10.1088/1361-6463/50/2/025304.

Sorkin, V. and Zhang, Y.W. (2016), "Mechanical properties of phosphorene nanotubes: a density functional tight-binding study", *Nanotechnology*, **27**, 395701. 10.1088/0957- https://doi.org/4484/27/39/395701.

Venkateshalu, S., Subashini, G., Bhardwaj, P., Jacob, G., Sellappan, R., Raghavan, V., Jain, S., Pandiaraj, S., Natarajan, V., Al Alwan, B.A.M. and Al Mesfer, M.K.M. (2022), "Phosphorene, antimonene, silicene and siloxene based novel 2D electrode materials for supercapacitors-A brief review", *J. Energy Storage*, **48**, 104027. https://doi.org/10.1016/j.est.2022.104027.

Wang, G., Loh, G.C., Pandey, R. and Karna, S.P. (2016), "Out-of-plane structural flexibility of phosphorene", *Nanotechnology*, **27**, 055701. https://doi.org/10.1088/0957-4484/27/5/055701.

Zhu, F., Yin, H., Wei, N. and Wan, J.(2020), "Numerical study of thermal conductivity based on phosphorene anisotropy: Including [110] direction and related phosphorus nanotubes", *Materialstoday*, **22**, 100814. https://doi.org/10.1016/j.mtcomm.2019.100814.

Zhi, C., Bando, Y., Tang, C., Kuwahara, H. and Golberg, D. (2009), "Large-scale fabrication of boron nitride nanosheets and their utilization in polymeric composites with improved thermal and mechanical properties", *Adv. Mater.*, **21**, 2889-2893. https://doi.org/10.1002/adma.200900323.

SR